Flow instabilities development inside an open cavity

Thierry Faure, Audrey Defrasne, François Lusseyran, Luc R. Pastur

FLOW INSTABILITIES DEVELOPMENT INSIDE AN OPEN CAVITY

Thierry M. Faure*,, Audrey Defrasne*,***, François Lusseyran*, Luc R. Pastur*,***
* LIMSI, B.P. 133, 91403 Orsay Cedex, France
** Université Pierre et Marie Curie, 4 place Jussieu, 75252 Paris Cedex 05, France
*** Université Paris-Sud, 91405 Orsay Cedex, France**

KEYWORDS:
Main subject: *Optical Technique*
Fluid: *Aerodynamics*
Visualization methods: *Particle Image Velocimetry (PIV), Tracer emission*

ABSTRACT : *The interaction between a laminar boundary layer and a rectangular cross-sectional cavity is studied with tracer injection visualizations and particle image velocimetry (PIV) in different planes of observation. Flow dynamics inside the cavity is driven by the shear layer, developing above the cavity, and a main vortex, developing along the whole cavity span. Secondary vortices are also present for some cavity geometries. 3D flow morphology is confirmed by tracer injection and PIV velocity streamlines. Transverse flows show low-velocity loops from the cavity centerline towards the lateral sides. For some Reynolds numbers and geometries, pairs of counter-rotating vortices are appearing, superimposed to the transverse flow. They are identified on both tracer injection visualizations and PIV measurements. The investigation of a wide range of parameters gives the thresholds for the appearance and disappearance of such centrifugal instabilities which are resulting from the imbalance between centrifugal forces and radial pressure gradient inside the main cavity vortex. The PIV field leads to the measurement of the momentum thickness and advection velocity inside the cavity, allowing a representation in a stability diagram.*

1 General Introduction

Flow over open cavity is a benchmark case for numerous industrial issues with structural discontinuities. A complete bibliographical analysis of this type of flow for compressible and incompressible conditions is available [1]. This experimental study reports the flow developments inside a parallelepipedic cavity of variable shape and dimensions. That flow is generated by the interaction between a laminar boundary layer and a cavity which creates self-sustained oscillations. The Reynolds number built on the external flow velocity and the cavity length is between 860 and 32 300, and the Mach number is lower than 0.01 so the flow is considered incompressible. The aim is the understanding of the 3D flow morphology varying the Reynolds number and the cavity shape. Flow visualizations and PIV measurements are obtained in different laser planes in order to get the dynamical structures. The main flow morphology and 3D developments are described with respect to cavity geometry and Reynolds number. The existence of eddy instabilities of the type of Görtler vortices [2,3] is identified for some cases. Thresholds and features of these instabilities are determined from measurements.

2 Experimental set-up and apparatus

The airflow is generated by a centrifugal fan placed upstream of a settling chamber (Figure 1-a). The seeding particle injection is achieved at the fan inlet. An axial duct terminated with honeycomb and a contraction drives the flow towards the experimental facility, which consists of a test section containing a flat plate beginning with an elliptical leading edge, in order to fix the boundary layer origin. The length of the plate is $A = 300$ mm providing an established laminar boundary layer at the cavity upstream edge. To reduce light wall reflections, the whole test section is made of antireflection glass 2 mm in thickness. The cavity height is varied between $H = 25$ mm and $H = 150$ mm. Its span $S = 300$ mm is constant because the cavity ends in this direction are the wind tunnel vertical walls (Figure 1-b). In addition to the Reynolds number, two other dimensionless numbers are defined: the span ratio as $F = S / H$ (span over height) studied from 2 to 12 and the cavity aspect ratio $R = L / H$ (length over height) from 0.25 to 2.5. This latter ratio can be changed continuously by moving the glass pieces consisting in the downstream wall of the cavity and the downstream plate, which has a length $B = 370$ mm. At the wind tunnel outlet, the flow is rejected inside the experimental room. The Reynolds number, determined with the cavity length L and the upstream boundary layer external velocity U_e, varies from 860 to 32 300, corresponding to external velocities from 0.57 to 3.68 $\mathrm{m \cdot s^{-1}}$. The external velocity is measured with laser Doppler velocimetry 102 mm upstream of the cavity and 25.5 mm above the flat plate. This point of measurement is in the external flow sufficiently upstream of the cavity to avoid any perturbation from the instability developing above the cavity. The origin of the coordinate system is set at the upstream edge of the cavity at mid span, the x axis is the flow direction, the y axis is normal to the upstream wall where the boundary layer develops and the z axis is along the cavity span. It has been checked that the test section upper wall, located at $D = 75$ mm above the cavity, has no influence on the shear layer developing on the cavity and, as a consequence, no influence on the flow. The thickness of the boundary layer developing on this wall is less than 10 mm and has no influence on the external flow along the longitudinal and spanwise directions. It has been shown for backward facing step flows that the influence of the upper wall affects the flow from 10 cavity heights downstream of the beginning of the step. The cavity under investigation is not a shallow cavity ($L / H > 5$), where the shear layer tends to attach the cavity floor. However, in that configuration, the development and propagation of the large-scale vortices appear to be relatively unaffected by confinement effects. In the present study, it will be even more so given the maximum aspect ratio of 2.5.

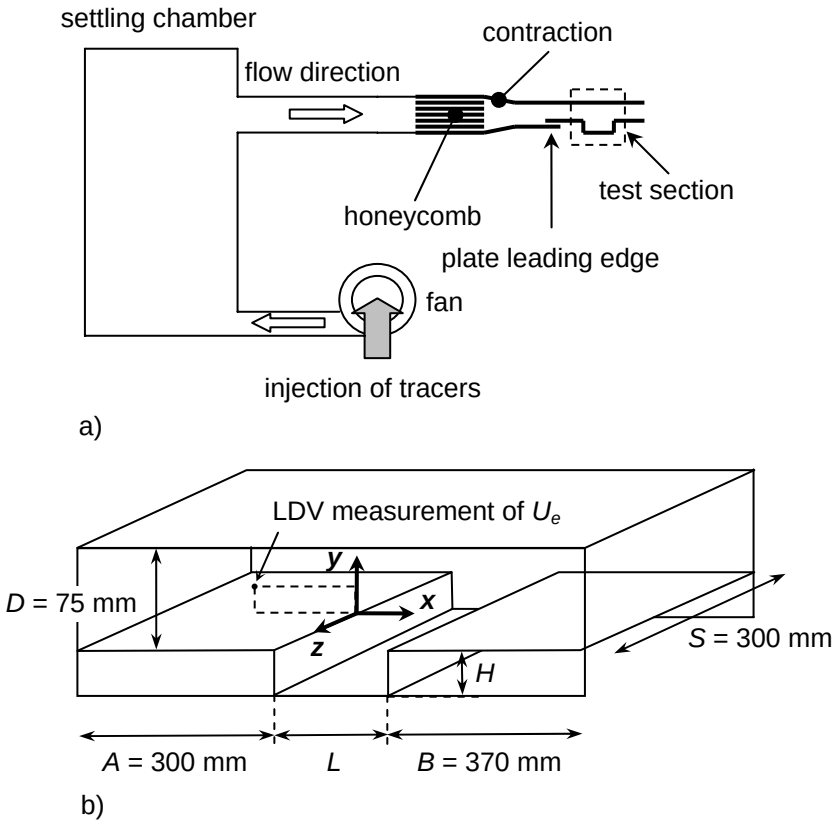

Figure 1: Experimental set-up: a) wind tunnel, b) test section dimensions and coordinate system.

Hereafter, the expressions “upstream” and “downstream” will refer to the external velocity direction. Flow visualizations by tracer injection are carried out with fog obtained with a low density smoke generator. As a result, the observed structures are emission lines of fluid injection inside the cavity and not the streamlines themselves. However, the flow injection inside the cavity gives information on the flow dynamics and the developing structures. The light source is a 5 W argon-ion laser tuned to the blue wavelength (488 nm). The laser beam provides, by passing through a cylindrical lens, a sheet whose thickness is 0.25 mm. The image recording system consists of a 10-bit camera with 1 032×778 pixels and a frequency of 20 Hz. The repeatability of flow visualizations has been checked by recording different image series with different wind tunnel runs, and by testing different smoke injections. The external flow is established and uniformly seeded with smoke when the images are recorded. Note that if the observation time is too long, there is a saturation of the cavity with smoke and no dynamical flow pattern can be identified anymore. PIV measurements are carried out with a pulsed YAG laser emitting in the 532 nm wavelength a sheet with a maximum thickness of 0.25 mm. The camera used for image recording is the same as for flow visualizations. The velocity fields are processed through a technique that uses an optical flow algorithm with dynamical programming, which provides high resolution fields (1 vector per pixel) particularly accurate for regions of high velocity gradients as shear layers. The corresponding velocity resolution is 1 / 32th pixel or a relative velocity accuracy of 0.15 % [4]. Hereafter, results are shown for two observation planes: a (x,y) plane providing information on the main flow morphology, and a (x,z) plane, providing information on the secondary instabilities (Figure 2). In each configuration, the camera has a complete view of the cavity length or

span. For the first observation direction, the (x,y) plane is set at cavity midspan. For the second observation direction, the (x,z) plane is set to a relative vertical position $y^* = y / H = -0.3$.

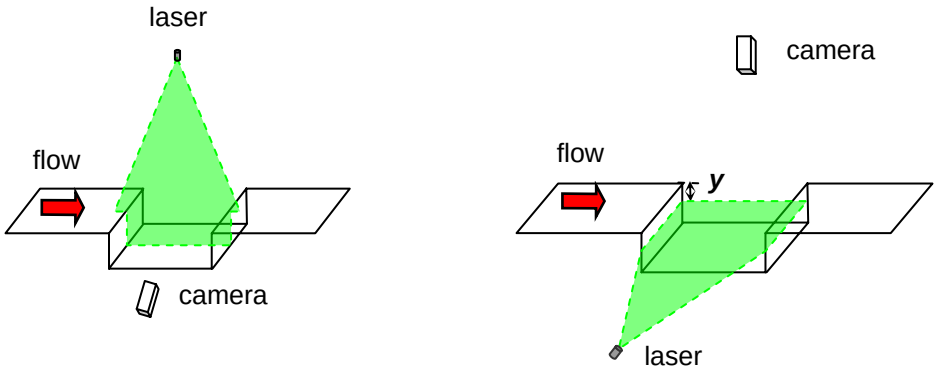

a) b)

Figure 2: Visualization inside a) a (x,y) plane or b) a (x,z) plane inside the cavity.

3 Cavity flow morphology

The velocity gradient produced by the interaction between the external flow and the cavity generates a shear layer characterized by the development of an oscillating wave. For the Reynolds number range under investigation, the starting point of the oscillations is not generally the upstream edge of the cavity [5]. In addition, there is no emission of vortices from this edge, contrary to what happens for higher Reynolds numbers, for instance in compressible flows [6]. According to the aspect ratio and for $F = 6$, different flow morphologies can develop inside the cavity, driven by one or several vortices. For $R = 2$ the flow exhibits a main clockwise vortex, located in the downstream part of the cavity and spreading over $2 L / 3$ (Figure 3). A secondary counter-rotating vortex is unevenly present in the upstream part of the cavity. For $R = 1.5$, the flow morphology is similar with a lower extension of the main vortex and secondary vortex, the latter being limited to the bottom of the cavity. For $R = 1$, only the clockwise vortex remains, with two small corner vortices. For $R = 0.5$, the clockwise vortex vertical extension is reduced to $H / 2$ while a counter-rotating vortex with very low velocity is present in the bottom of the cavity. This morphology is confirmed by the streamlines of the velocity field (Figure 4). For these PIV measurements, a judicious choice of the measurement parameters allows a good description of both the external and cavity flows, while the maximum velocities inside the cavity are $1 / 10^{th}$ of the external velocity. Note that the aspect ratio is the only controlling parameter and that the Reynolds number has no influence at all on that vortex morphology. It has just an influence on their stability. The three-dimensional character of the cavity flow has been recognized in previous studies [1,2,3,7,8]. The span confinement of the cavity induces recirculating flows, as it can be seen in a (x,z) plane in Figure 5, forming four recirculation cells. These transverse flows show low-velocity loops from the cavity centerline towards the lateral sides. That flow superimposes with the spanwise vortex dynamics previously described.

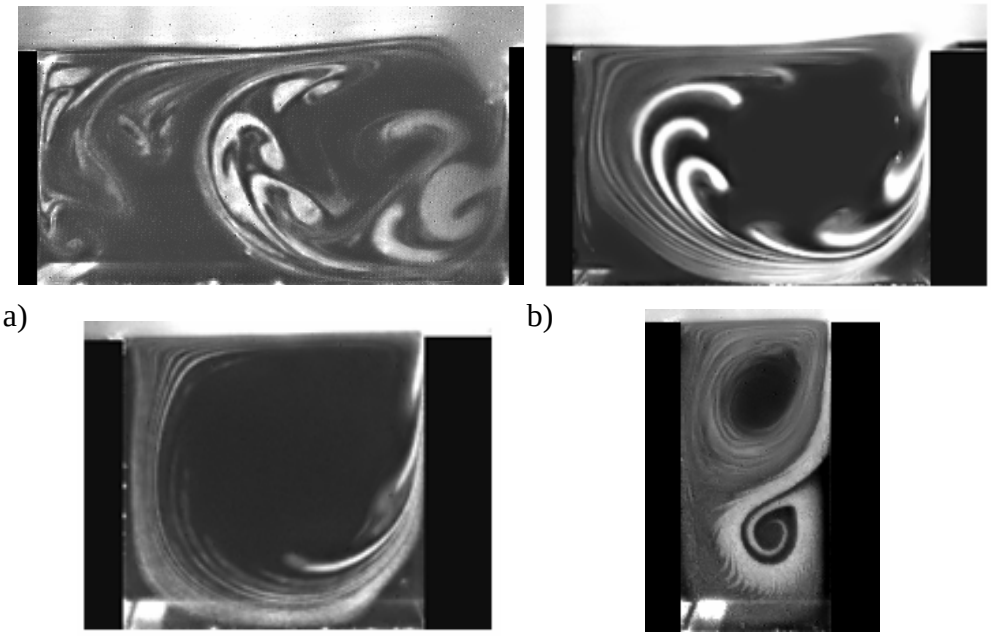

a) b) c) d)

Figure 3: Flow visualizations for a) R = 2, b) 1.5, c) 1 and d) 0.5, F = 6 and Re between 5 933 and 1 483.

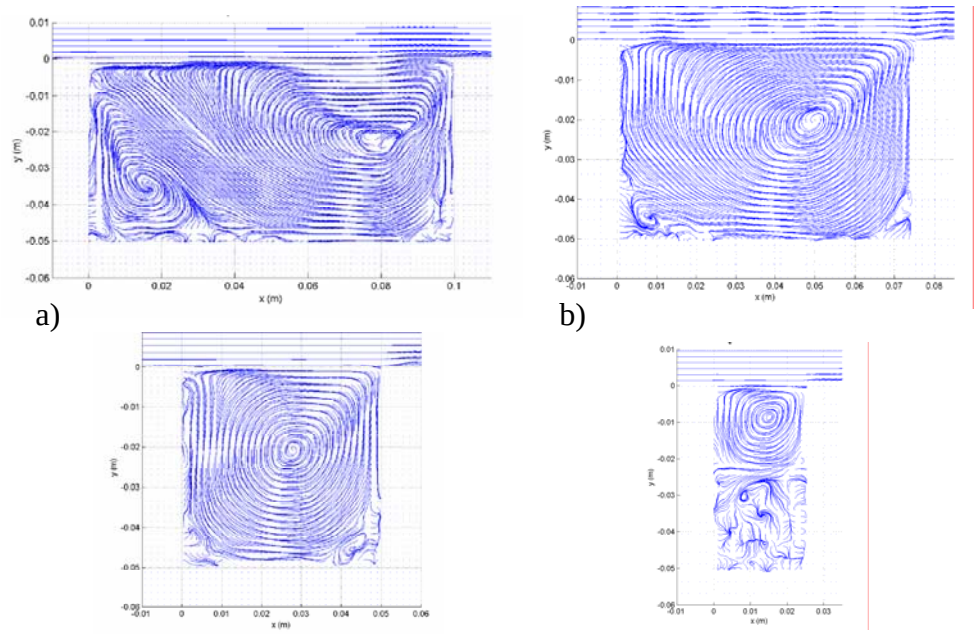

a) b) c) d)

Figure 4: Flow streamlines for a) R = 2, b) 1.5, c) 1 and d) 0.5, F = 6 and Re between 5 933 and 1 483.

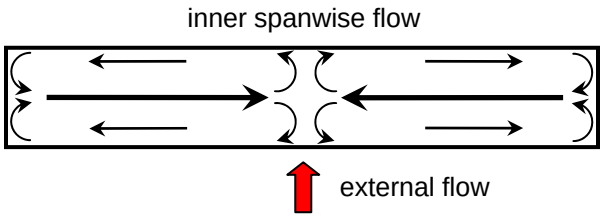

Figure 5: Sketch of transverse flow.

4 Development of centrifugal instabilities

This part is focusing on the particular cases where centrifugal flow instabilities of Görtler type are superimposed with the flow morphology depicted in the previous section. They have been identified in separated flow [2,9]. Their existence and properties are discussed in relation with the Reynolds number, aspect ratio and span ratio. If the Reynolds number is high enough, a spanwise row of counter-rotating pairs appears near the upstream and downstream walls (Figure 6 and Figure 7). In fact, these pairs of instabilities form a succession of loops inscribed inside the cavity (x,y) planes. For some cases, single pairs are also identified, generally near the upstream edge of the cavity where there is no interaction between the main vortex and the shear layer oscillations (Figure 8) but they do not show a loop-like shape. It seems that the key mechanisms of the instabilities birth are a large enough advection velocity, generated by the main spanwise vortex, and a large enough curvature radius. Their destruction is linked to the flow transition to turbulence above a limiting velocity. Configurations with no instability are present, generally where the advection velocity is not sufficient to destabilize the wall boundary layers.

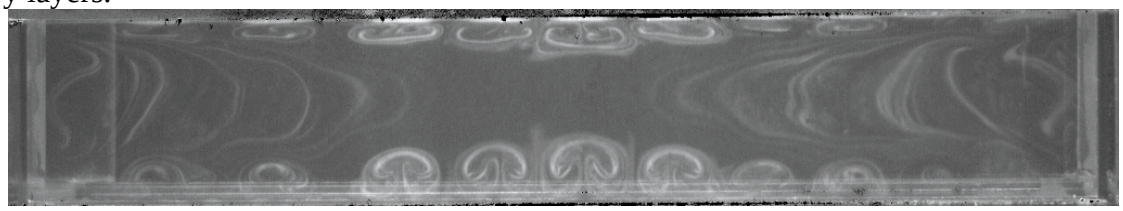

Figure 6: Flow visualization of counter-rotating instabilities for R = 1, F = 6 and Re = 4 233.

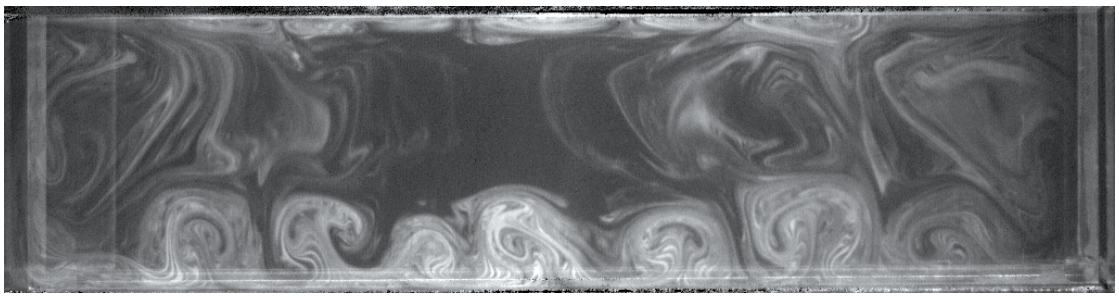

Figure 7: Flow visualization of counter-rotating instabilities for R = 1.5, F = 6 and Re = 4 450.

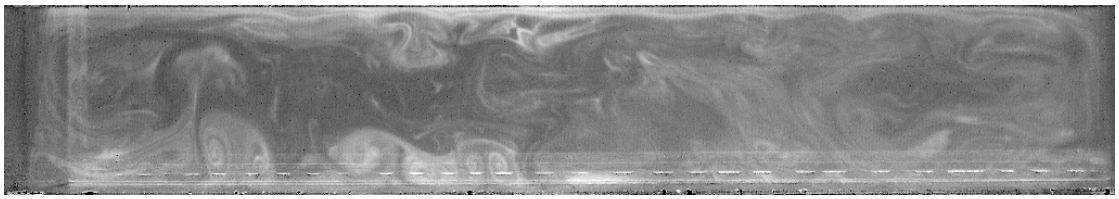

Figure 8: Flow visualization of counter-rotating instabilities for R = 0,5, F = 3 et Re = 7 500.

These instabilities are also identified on PIV measurements (Figure 9) despite the high velocity component perpendicular to the plane of measurement. The instabilities rows are identified in the y component of the vorticity field showing high positive and negative levels near the upstream and downstream cavity edges (Figure 10). A careful examination of this figure proves the annular shape of these centrifugal instabilities in the (x,y) plane, with the extension of the blue and yellow regions along the x direction.

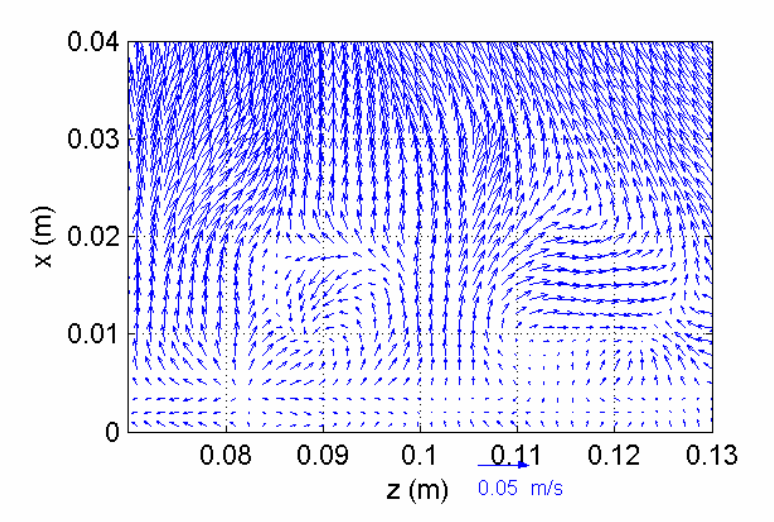

Figure 9: PIV measurement of counter-rotating instabilities for R = 1.5, F = 6 and Re = 4 450.

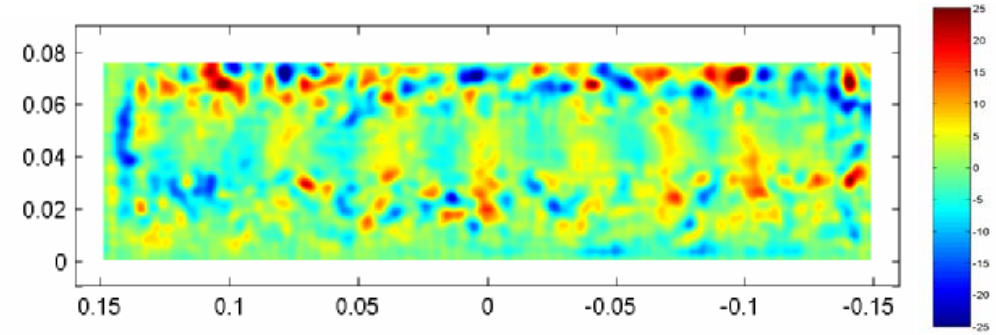

Figure 10: Y-component of the vorticity of the velocity field for R = 1.5, F = 6 and Re = 4 450.

It must be noticed that such pairs of instability vortices are the most robust when only one main vortex exists within the cavity. Indeed, as soon as the secondary vortex appears, the Görtler-like vortices are stretched and dislocate. This is suggesting that the cavity aspect ratio range for their existence should be around R = 1. For larger aspect ratios, the structures are also present but the key mechanism of their existence domain is a combination of geometry (R and F) and Re. An extensive study has been

conducted varying the external flow velocity, cavity length and height, and, as a consequence, *Re*, *R* and *F*. Figure 11 shows the domain of existence of centrifugal instabilities, as functions of Reynolds number and aspect ratio, for different span ratios. The region where these instabilities are present in the plane (*R*, *Re*) is forming a compact domain, which tends to prove the existence of limiting thresholds for their birth and vanish. For some cases and small values of the span ratio (*F* = 3 and 2), instead of a row of vortices there is a single Görtler vortex near the upstream cavity edge. For these configurations, the vortex does not form a loop inside the cavity.

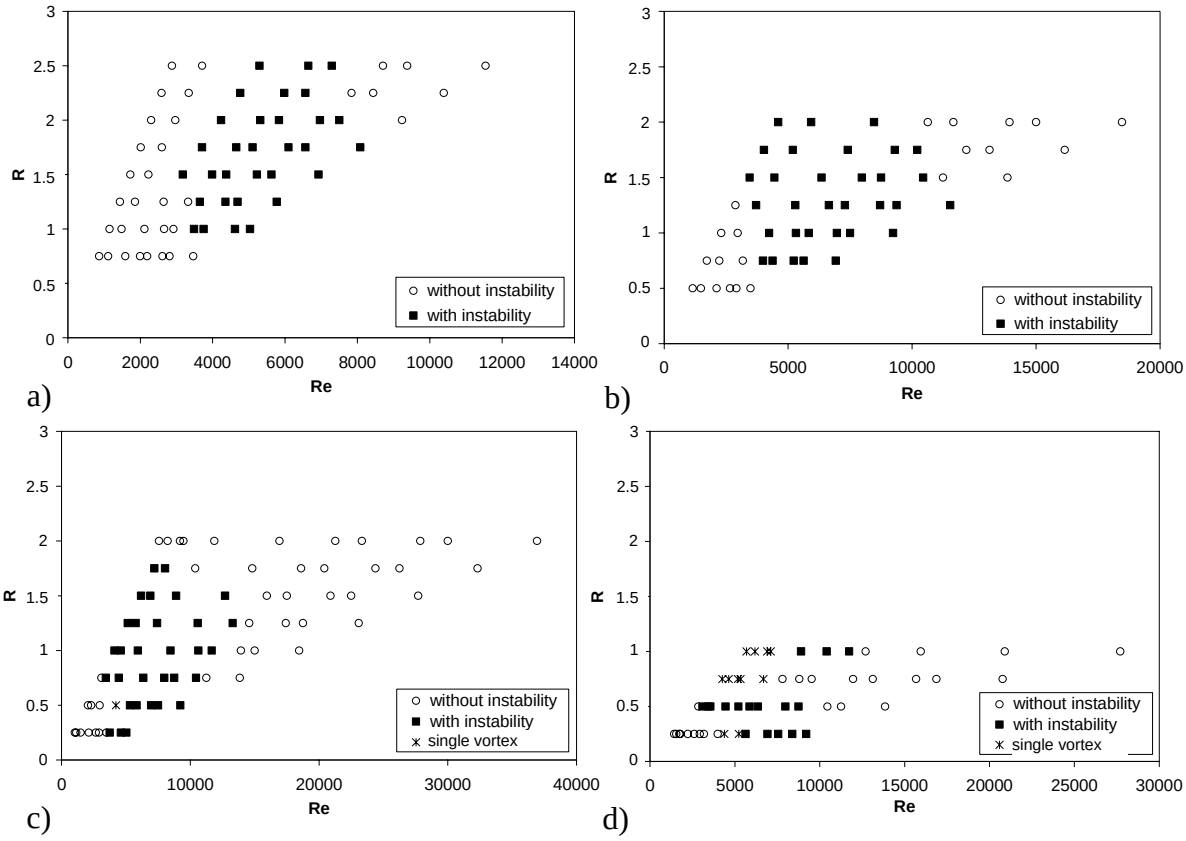

Figure 11: Existence diagram of centrifugal instabilities a) *F* = 12, b) *F* = 6, c) *F* = 3 et d) *F* = 2.

Figure 12 show the number of Görtler vortices present simultaneously inside the measurement plane, for configuration exhibiting rows of these instabilities. For each span and aspect ratio, we note an increase followed by a decrease of the pairs of vortices number versus the Reynolds number. This is the proof that the appearance-vanish cycle is a continuous phenomenon driven by the external velocity U_e. The geometry is also important since there is an aspect ratio for which the vortices number reaches a maximum. We can notice in Figure 12-a and Figure 12-b that this maximum number of pairs of vortices is found for *R* = 1. This can be understood as the presence of a main circular vortex inside the cavity, which provides a best radius of curvature with respect to wall confinement. There is a drop of the number of vortices for *F* = 3 (Figure 12-c). The same comment is done for *F* = 0.5 with a lower number of vortices (Figure 12-d). That decrease in the number of vortices inside the cavity with span ratio shows that the lateral flow confinement could be opposed to the development of centrifugal instabilities.

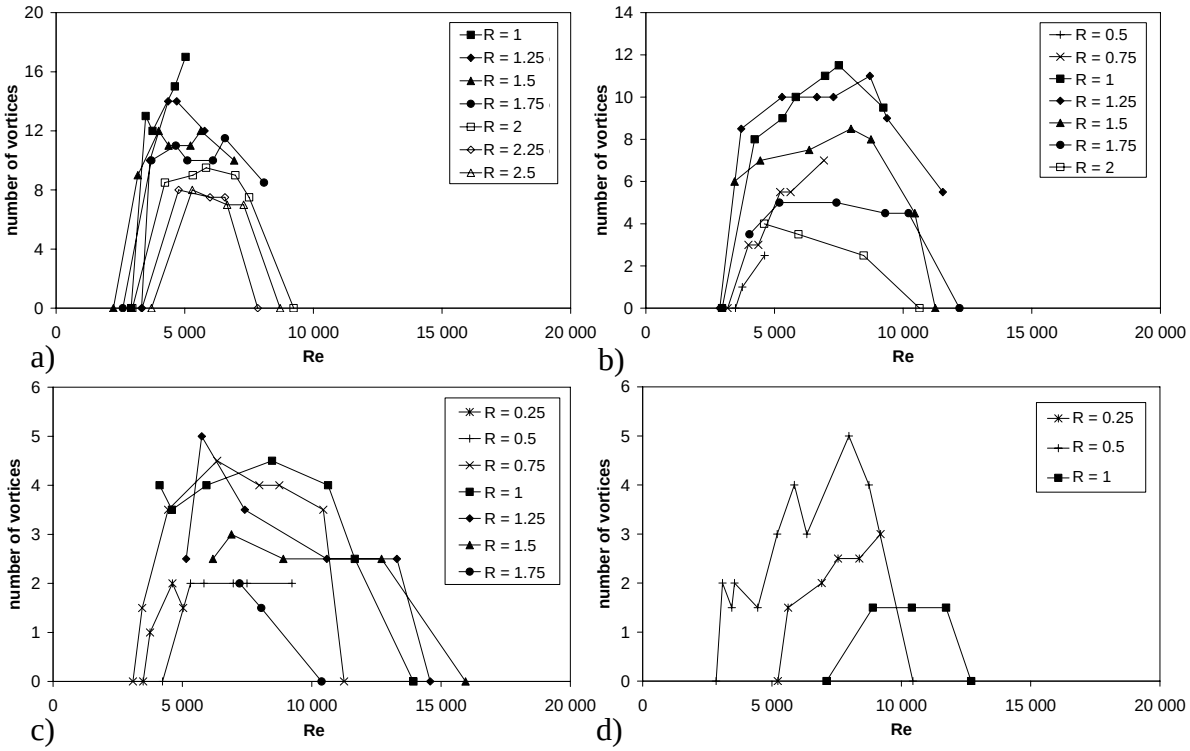

Figure 12: Number of centrifugal instabilities a) F = 12, b) F = 6, c) F = 3 et d) F = 2.

The flow curvature caused by the main vortex is thought to be the key mechanism of the development of centrifugal instabilities. That hypothesis is consistent with quantitative results on the spanwise primary instability [10]. The Görtler number, defined with the curvature radius r_c, the kinematics viscosity of the fluid $\nu = 15\times10^{-6}$ m^2·s^{-1} and the velocity inside the cavity U_c developing away from the boundary layer of momentum thickness δ_2 is:

$$G\ddot{o} = \frac{U_c \delta_2}{\nu}\left(\frac{\delta_2}{r_c}\right)^{\frac{1}{2}} \qquad (1)$$

The Görtler number actually compares the local curvature of the flow with the viscosity effects. The wave number k is defined as:

$$k = \frac{2\pi}{\lambda} \qquad (2)$$

where the wavelength λ is the distance between two pairs of counter-rotating patterns. In the present case, U_c, δ_2 and k are obtained from PIV measurements in a (x,y) plane (Figure 4). When the Görtler number is high enough, the curvature effects dominates the viscosity effects and the flow is unstable, leading to centrifugal instabilities. Reporting the Görtler number versus the dimensionless wave number $k\,\delta_2$ on the stability diagram (Figure 13) we observe a good agreement between our estimates and previous measurements [11,12,13]. Comparison is made with the neutral stability curve [14] and all the measurement points are on the left of this curve, corresponding to the instable region.

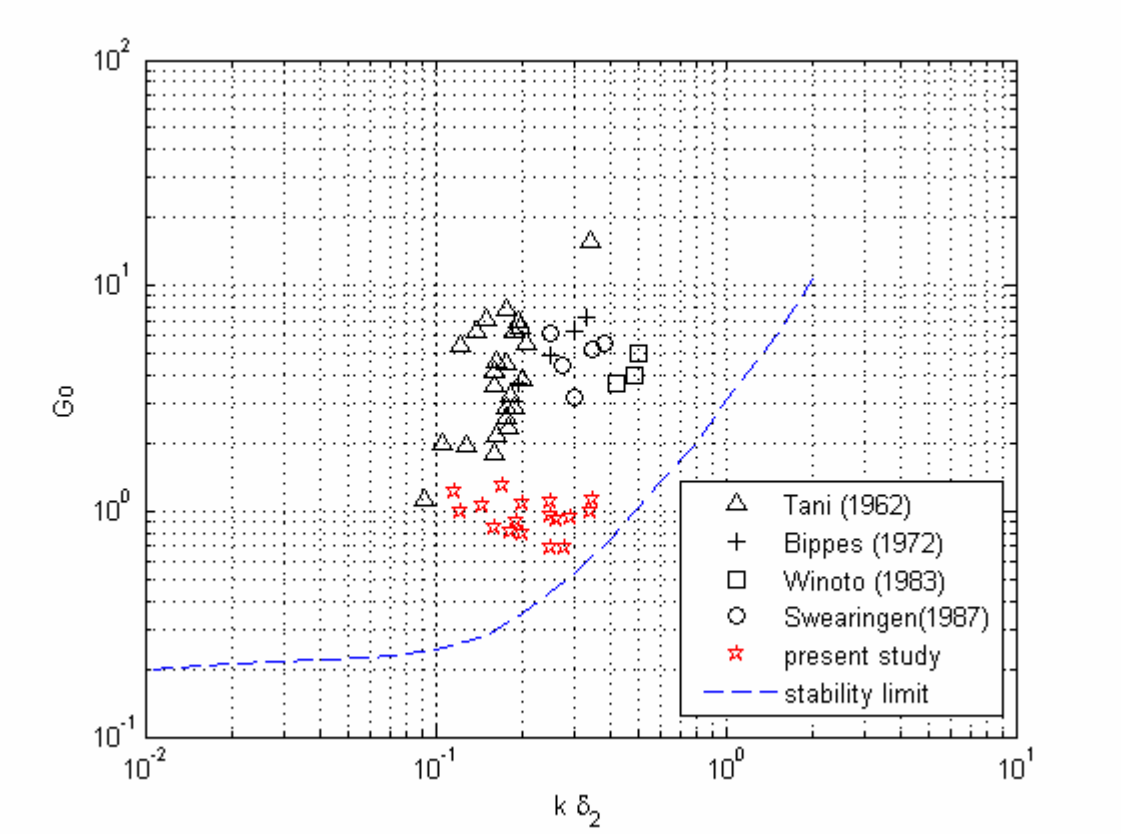

Figure 13: Stability diagram of centrifugal instabilities.

5 Conclusion

The interaction between a laminar boundary layer flow and a cavity of variable dimensions is studied for a range of medium Reynolds numbers with tracer emission visualization and PIV. The flow morphology is driven by a shear layer which induces one or several cavity vortices according to the geometry. The main vortex is, for a limited range of Reynolds number and geometrical parameters, the generating mechanism of secondary centrifugal instabilities. They form a row of pairs of counter-rotating vortices with an annular shape inscribed inside the cavity cross-section. For some cases, single pairs of Görtler vortices are also present. It seems that the key mechanisms of the instability birth are a large enough advection velocity, generated by the main spanwise vortex, and a large enough curvature radius. Such pairs of instability vortices are the most robust when only one main vortex exists within the cavity. The domain of existence of centrifugal instabilities has been established, proving the existence of limiting thresholds for their birth and vanish. A perspective to this work is the implementation of stereoscopic PIV in order to measure the third velocity component, which is expected to be dominant in the Görtler vortex core.

6 References

1. Faure T M, Adrianos P, Lusseyran F, Pastur L R. Visualizations of the flow inside an open cavity at medium range Reynolds numbers. *Experiments in Fluids*, Vol. 42, No. 2, pp. 169–184, 2007.

2. Migeon C. Details on the start-up development of the Taylor-Görtler-like vortices inside a square-section lid-driven cavity for 1,000 ≤ Re ≤ 3,200. *Experiments in Fluids*, Vol. 33, pp. 594–602, 2002.
3. Migeon C, Pineau G, Texier A. Three-dimensionality development inside standard parallelepipedic lid-driven cavities at Re = 1000. *Journal of Fluids and Structures*, Vol. 17, pp. 717–738, 2003.
4. Faure T M, Lusseyran F, Gougat P, Launay F. Experimental investigation of the flow distribution inside a tubular heat exchanger, *Journal of Fluids Engineering*, Vol. 128, No 6, pp. 1218–1227, 2006.
5. Faure T M, Lusseyran F, Pastur L R, Pethieu R, Debesse P. 2006 Développement d'instabilités dans un écoulement subsonique se développant au-dessus d'une cavité : mesures synchronisées PIV-LDV, *10ème Congrès Francophone de Techniques Laser*, Toulouse, pp. 577–584, 2006.
6. Forestier N, Jacquin L, Geffroy, P. The mixing layer over a deep cavity at high-subsonic speed. *Journal of Fluid Mechanics*, Vol. 475, pp. 101–145, 2003.
7. Faure T M, Debesse P, Lusseyran F, Gougat P. Structures tourbillonnaires engendrées par l'interaction entre une couche limite laminaire et une cavité, *11ème Colloque de Visualisation et de Traitement d'Images en Mécanique des Fluides*, Lyon, 2005.
8. Guermond J L, Migeon C, Pineau G, Quartapelle L. Start-up flows in a three-dimensional rectangular driven cavity of aspect ratio 1:1:2 at Re = 1000, *Journal of Fluid Mechanics*, Vol. 450, pp. 169–199, 2002.
9. Beaudoin J F, Cadot O, Aider J L, Wesfreid J E. Three-dimesional stationary flow over a backward-facing step, *European Journal of Mechanics B/Fluids*, Vol. 23, pp. 147–155, 2004.
10. Swearingen J D, Blackwelder R F. The growth and breakdown of streamwise vortices in the presence of a wall, *Journal of Fluid Mechanics*, Vol. 182, pp. 255–290, 1987.
11. Tani I. Production of longitudinal vortices in the boundary layer along a concave wall, Journal of Geophysical Research, Vol. 67, pp. 3075–3080, 1962.
12. Bippes H. Experimentelle Untersuchung des laminar-turbulenten Umschlags an einer parallel angeströmten könkaven Wand, *Heidel. Akad. Wiss. Naturwiss. Kl.*, Vol. 3, p. 103, 1972.
13. Winoto S H, Crane R I. Vortex structure in laminar boundary layers on a concave wall, *International Journal of Heat and Fluid Flow*, Vol. 2, pp. 221–231, 1980.
14. Floryan J M, Saric W C. Stability of Görtler vortices in boundary layers, *AIAA Journal*, Vol. 20, No. 3, pp. 316–324, 1982.

7 Movies

Movie 1: Cavity flow in a (x,y) plane for R = 2, F = 6 and Re = 8 466.
Movie 2: Cavity flow in a (x,y) plane for R = 1, F = 6 and Re = 4 233.
Movie 3: Centrifugal instabilities development in a (x,z) plane for R = 1, F = 6 and Re = 4 233.

Copyright Statement